Geophysical Prospecting, 2002, **50**, 15–25

Imaging magnetic sources using Euler's equation

Shu-Kun Hsu*

Institute of Geophysics, National Central University, Taiwan

Received April 2000, revision accepted May 2001

ABSTRACT

The conventional Euler deconvolution method has the advantage of being independent of magnetization parameters in locating magnetic sources and estimating their corresponding depths. However, this method has the disadvantage that a suitable structural index must be chosen, which may cause spatial diffusion of the Euler solutions and bias in the estimation of depths to the magnetic sources. This problem becomes more serious when interfering anomalies exist. The interpretation of the Euler depth solutions is effectively related to the model adopted, and different models may have different structural indices. Therefore, I suggest a combined inversion for the structural index and the source location from the Euler deconvolution, by using only the derivatives of the magnetic anomalies. This approach considerably reduces the diffusion problem of the location and depth solutions. Consequently, by averaging the clustered solutions satisfying a given criterion for the solutions, we can image the depths and attributes (or types) of the causative magnetic sources. Magnetic anomalies acquired offshore northern Taiwan are used to test the applicability of the proposed method.

INTRODUCTION

Techniques using potential field derivatives to image subsurface magnetic or gravity source geometry, such as locations and depths, draw more and more attention. Among these, the analytic signal and Euler deconvolution techniques are widely used (e.g. Nabighian 1972, 1974, 1984; Atchuta Rao, Ram Babu and Sanker Narayan 1981; Thompson 1982; Sundararajan *et al*. 1985; Hansen, Pawlowski and Wang 1987; Reid *et al*. 1990; Roest, Verhoef and Pilkington 1992; MacLeod, Jones and Dai 1993; Marson and Klingele 1993; Hsu, Sibuet and Shyu 1996; Ravat 1996; Debeglia and Corpel 1997; Thurston and Smith 1997; Hsu, Coppens and Shyu 1998; Keating 1998; Smith *et al*. 1998; Barbosa, Silva and Medeiros 1999). The main advantage of using the two techniques is that identified locations and depths to the causative sources are independent of magnetization directions. To the author's knowledge, the analytic signal method has attained, to some extent, the ability of recognizing the source attributes of simple forms, such as thin sheet (or thin dike), contact and cylinder structures (e.g. Hsu *et al*. 1998; Smith *et al*. 1998). Barbosa *et al*. (1999) provided a means of estimating a structural index but this requires (probably manual) isolation of individual anomalies. Fully automatic Euler deconvolution still suffers from the critical problem of choosing an appropriate structural index to estimate the source parameters. Unfortunately, a poor choice of structural index can cause diffused solutions of source locations and serious bias in depth estimation. This problem becomes serious when the magnetic anomalies from two or more sources interfere; for example, when two structures having different structural indices are close to each other. In fact, interfering anomalies are more or less inevitable in real data.

The structural index is a measure of the rate of change with distance of a field (Reid *et al*. 1990). In other words, this parameter provides information on the geometry of a causative body (Table 1). Thus, we should estimate the structural indices when we estimate the locations and depths of the causative sources from a field anomaly, rather than giving a structural index prior to applying the Euler deconvolution.

*E-mail: hsu@oc.gep.ncu.edu.tw

Table 1 Relationship between structural index (*N*), type of magnetic model and position of the calculated depth

N	Type of magnetic model	Position of Euler depth relative to the model
0	Contact or fault with small depth/throw ratio	At top and edge
1	Thin dike or fault with large depth/throw ratio	At top and centre, or at edge and half throw
2	Vertical or horizontal cylinder	At centre
3	Sphere	At centre

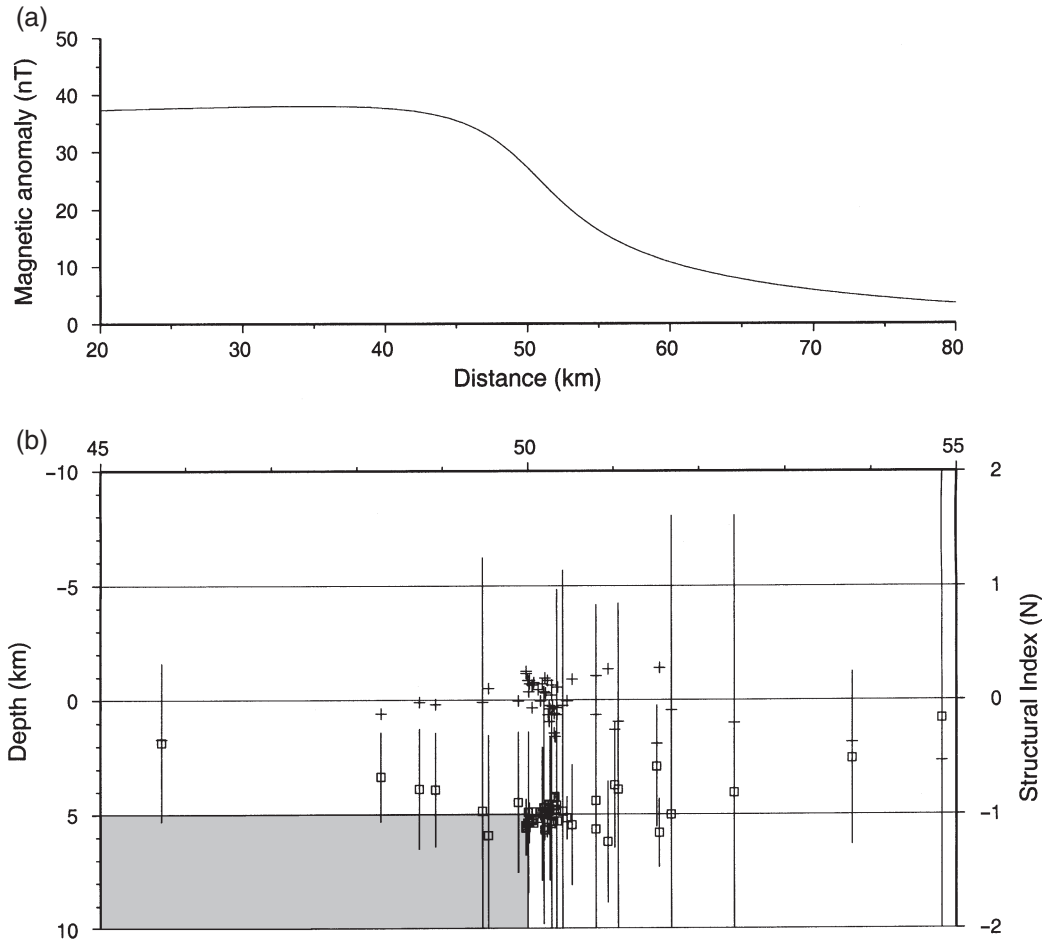

Figure 1 (a) Magnetic anomaly caused by a contact structure. The magnetization parameters are described in the text. (b) The calculated depth solutions (open squares) and structural indices (crosses) are obtained from the proposed method. One standard deviation of each depth solution is plotted on each side of a square. No selection criteria are applied to the solutions for the purpose of demonstration. Note that good depth solutions cluster at the top and edge of the model (shaded area) and good structural index solutions cluster around zero.

However, Euler's equation involves not only the derivatives of the potential field but also the field itself, and the absolute level of the field for a structure is rarely known (Thompson 1982). Consequently, a constant but unknown base level is commonly involved in the Euler deconvolution method. This situation results in the dependence of the structural index on the base level. For this reason, I suggest using only derivatives of field anomalies to image magnetic sources, when Euler's equation is used. This approach allows us to estimate a structural index for a magnetic anomaly, making the assumption that interfering gradients from adjacent bodies or regional effects are identically zero. Because the interpretation of the calculated depths obtained from Euler's equation depends on the attributes of the magnetic sources, an

appropriate estimation of the structural indices avoids ambiguous depth determination from clustering solutions.

THEORY

Thompson (1982) showed that Euler's homogeneity equation, when taking into account a base level for the background field, can be written as

$$(x-x_0)\frac{\partial M}{\partial x}+(y-y_0)\frac{\partial M}{\partial y}+(z-z_0)\frac{\partial M}{\partial z}=N(B-M), \qquad (1)$$

where M is the observed field at location (x, y, z) caused by a magnetic source at location (x_0, y_0, z_0), B denotes the base level of the observed field, and N denotes the structural index. The parameters N and B in (1) are obviously dependent on each other. For a valid determination of the structural index N, we take an nth-order vertical derivative for each term in (1). After some rearrangement, we obtain

$$(x-x_0)\frac{\partial}{\partial x}\left(\frac{\partial^n M}{\partial z^n}\right)+(y-y_0)\frac{\partial}{\partial y}\left(\frac{\partial^n M}{\partial z^n}\right)+(z-z_0)\frac{\partial}{\partial z}\left(\frac{\partial^n M}{\partial z^n}\right) = -(N+n)\frac{\partial^n M}{\partial z^n}. \qquad (2)$$

For the integer $n \geq 1$, (2) is independent of the base level B. Theoretically, (2) is valid when the nth-order vertical derivative of B is zero. For instance, when the background field B is constant, then $n \geq 1$ must be used; when $\partial B/\partial z \neq 0$ and $\partial^2 B/\partial z^2 = 0$ (i.e. the source is located on a sloping background), then $n \geq 2$ must be used. A non-constant magnetic background in fact is a common situation; for example, the earth's geomagnetic field is generally a minimum near the geomagnetic equator and it increases

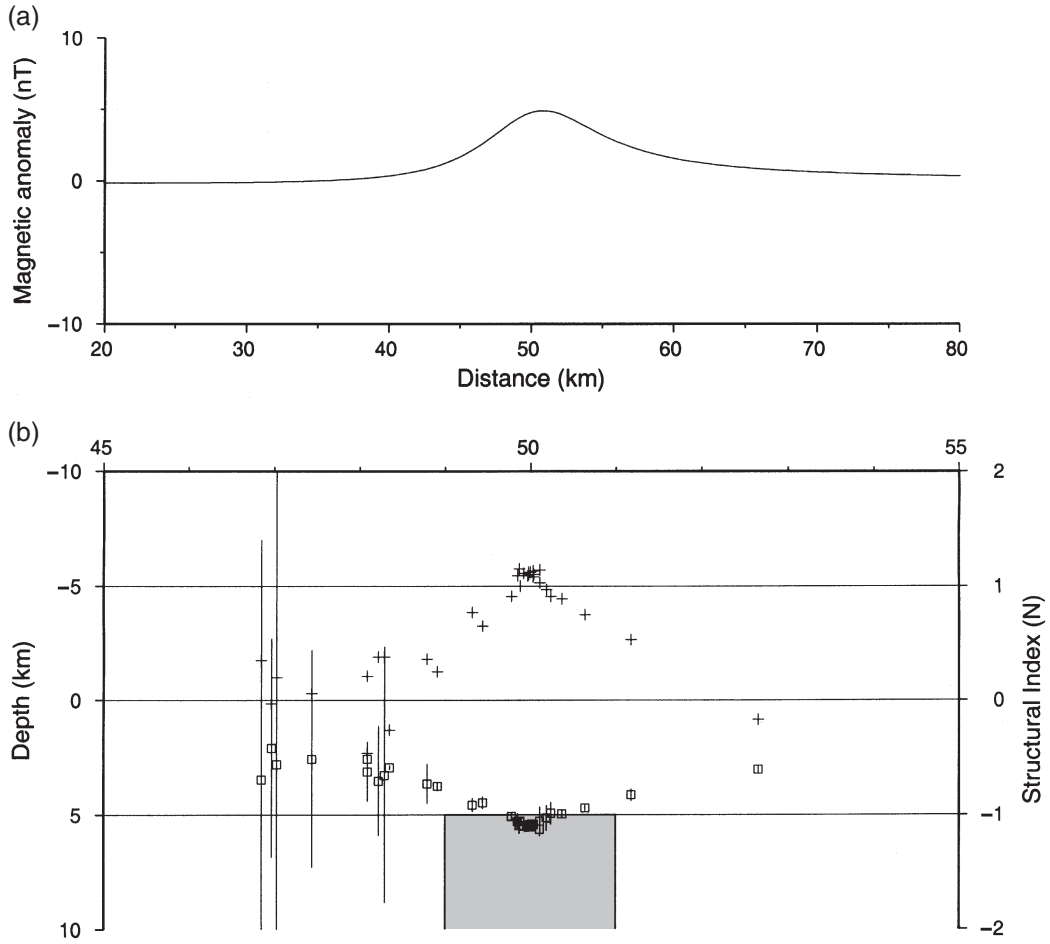

Figure 2 (a) Magnetic anomaly caused by a thin dike structure. Same magnetization parameters as in Fig. 1. (b) Solutions obtained from the proposed method. Solutions display is the same as in Fig. 1. Note that good depth solutions cluster at the top and centre of the model (shaded area) and good structural index solutions cluster around one.

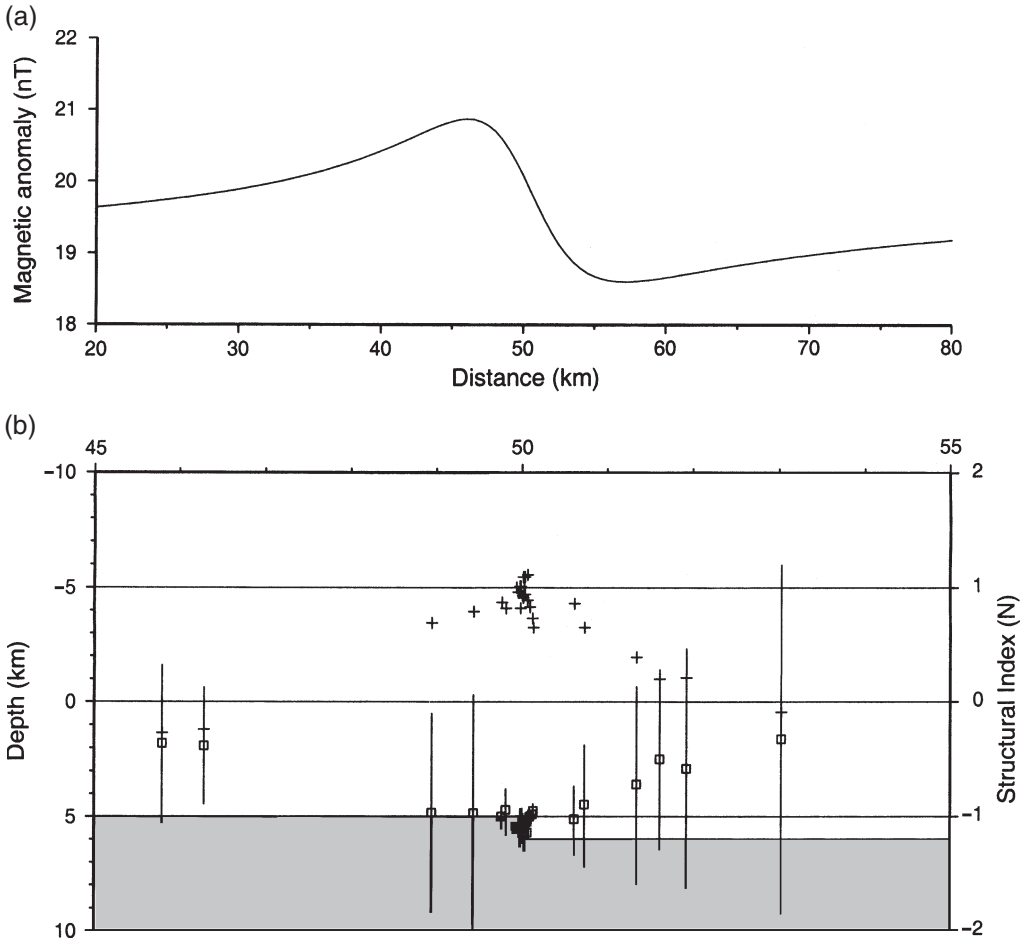

Figure 3 (a) Magnetic anomaly caused by a step structure with a large depth/throw ratio. Same magnetization parameters as in Fig. 1. (b) Solutions obtained from the proposed method. Solutions display is the same as in Fig. 1. Note that good depth solutions cluster at the midpoint of the throw of the model (shaded area) and good structural index solutions cluster around one.

gradually towards the geomagnetic poles. The components of the vertical or horizontal derivatives of the magnetic anomaly M in (2) could be obtained by numerical approximation (e.g. Hsu *et al.* 1996). Four unknowns, x_0, y_0, z_0 and N, remain to be determined. In general, four equations are sufficient to solve for the four unknowns. However, we can over-determine the four unknowns in the least-squares sense to obtain more reliable solutions. Therefore, in this study, four regularly spaced, consecutive points in a profile data set (for the 2D case) or a window of 4×4 grid nodes (for the 3D case) are adopted as an example. Both the first- and second-order vertical derivatives (i.e. $n=1$ and $n=2$ in (2)) of each data point are used in the following examples. To identify the good solutions for the location and attribute of a structure, three criteria have been used.

1 The uncertainty of each depth solution (i.e. z_0) must be limited. For example, Thompson (1982) kept solutions for which $z_0/N\sigma_z$ (i.e. the acceptance tolerance) is greater than 20, where σ_z is the standard deviation of the estimated depth. For convenience, we will use z_0/σ_z as the acceptance tolerance following the practice of Reid *et al.* (1990).

2 Good location solutions cluster at a structure.

3 Good structural index solutions also cluster at the correct structural index.

SYNTHETIC MODELS

2D model tests

Four 2D models are tested to demonstrate the applicability of the proposed method. The models consist of a contact model,

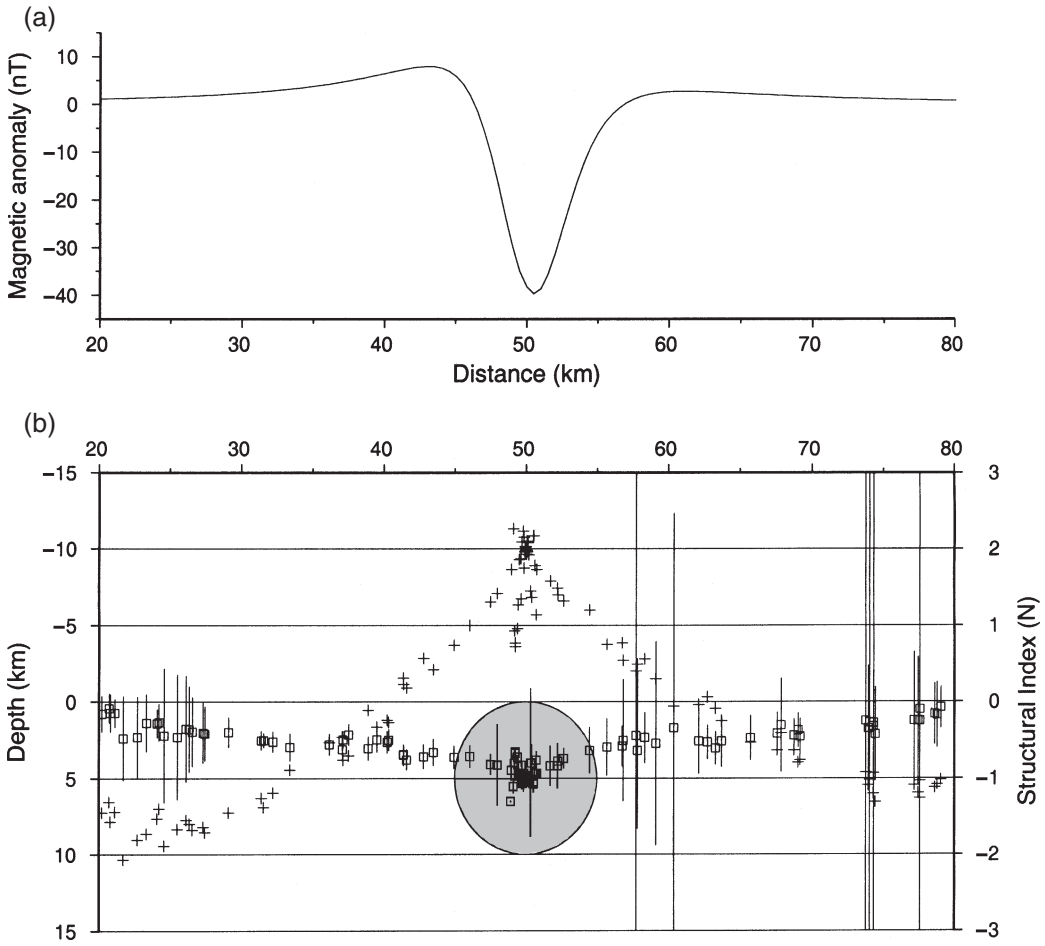

Figure 4 (a) Magnetic anomalies caused by a horizontal cylinder structure. Same magnetization parameters as in Fig. 1. (b) Solutions obtained from the proposed method. Solutions display is the same as in Fig. 1. Note that good depth solutions cluster at the centre of the model (shaded area) and good structural index solutions cluster around two.

a thin dike model, a fault model with large depth/throw ratio and a horizontal cylinder model. Their geometric shapes are shown in Figs 1(b)–4(b). For convenience, the magnetization intensity for each model is set at 2 A/m, and the magnetic declination and inclination are -5° and 30°, respectively. The grid spacing along the profile is 0.5 km. The corresponding magnetic anomaly for each model is illustrated in Figs 1(a)–4(a). It should be mentioned that only the magnetic total field anomalies are obtained by model calculation. The derivatives needed in (2) are calculated numerically, because derivatives (especially higher order) are seldom acquired in real surveys.

In Figs 1(b)–4(b), both good and bad solutions obtained from every four consecutive points (i.e. eight equations) along a profile are shown. For the purpose of discussion, selection criteria are not applied to the solutions; thus, we can see that good solutions are clustered for both the location and structural index solutions, while the incorrect solutions are diffused (Figs 1–4). Theoretically, a structural index is always greater than zero. The negative structural indices suggest wrong solutions and should be eliminated from the final results. However, taking into account some error from numerical approximation and noise, the estimated value of a structural index may be 'slightly less' than zero. A suitable structural index could be obtained by averaging the values within a clustered area. As shown in Figs 1(b)–4(b), the structural indices for a contact or a vertical step model with a small depth/throw ratio, a thin dike model, a fault model with large depth/throw ratio and a horizontal cylinder model are clustered about 0, 1, 1 and 2, respectively. These values are in agreement with the theoretical values of structural index shown in Table 1.

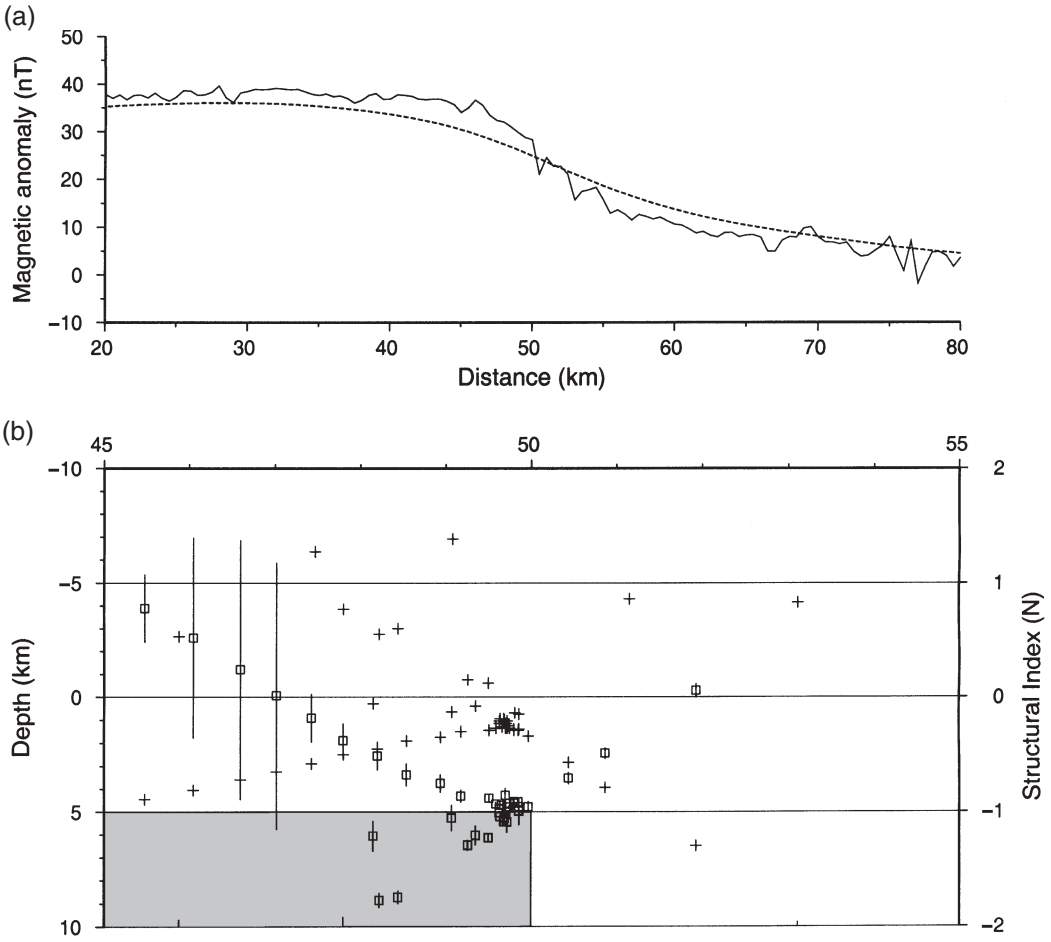

Figure 5 (a) Noisy magnetic data (solid line) which correspond to 30% noise in Fig. 1(a). The dashed line indicates an arbitrary 4 km upward continuation of the data. (b) Euler solutions obtained by using the proposed method. Solutions display is the same as in Fig. 1.

The calculated depths to each 2D model are shown in Figs 1(b)–4(b). The error bar within $\pm 1\sigma_z$ of the calculated depth is also plotted. It can be seen in Figs 1(b)–4(b) that the good depth solutions are clustered and display small standard deviations. However, we shall consider the interpretation of depth solutions. That is, we must interpret the depth solutions together with their associated structural indices. For example, in Fig. 1(b), the good depth solutions cluster at the top and the edge of the contact. For a thin dike model, the depth solutions, in contrast, cluster at the top and centre of the thin dike (Fig. 2b). For a vertical step fault, which has a large depth/throw ratio (Fig. 3b), the obtained depth is located at about the midpoint of the throw, rather than the top of the fault. For a horizontal cylinder, the depths of the clustered solutions are located at the centre of the cylinder (Figs 4b and 5). These 2D models indicate that the depths calculated using Euler's equation are not necessarily the depths to the tops of causative sources (Reid *et al.* 1990; Ravat 1996). Their depth interpretations depend on the geometric attributes of the structures. These tests reveal the importance of knowing the geometry of a magnetic source when Euler's equation is used to investigate the depth to the source.

Noisy data test

Noise in the magnetic anomaly of a magnetic source is more or less inevitable in real surveys. To test the noise influence on the proposed method, random noise with a range of about 10 nT is added to the noise-free magnetic anomaly in Fig. 1(a) (Fig. 5a). These noise-corrupted data correspond to about 30% noise in the magnetic anomaly. To ensure a stable calculation, the data are smoothed by upward continuation for an arbitrary 4 km (Fig. 5a). The Euler solutions shown in Fig. 5(b) are obtained by using (2) with $n=1$ and $n=2$.

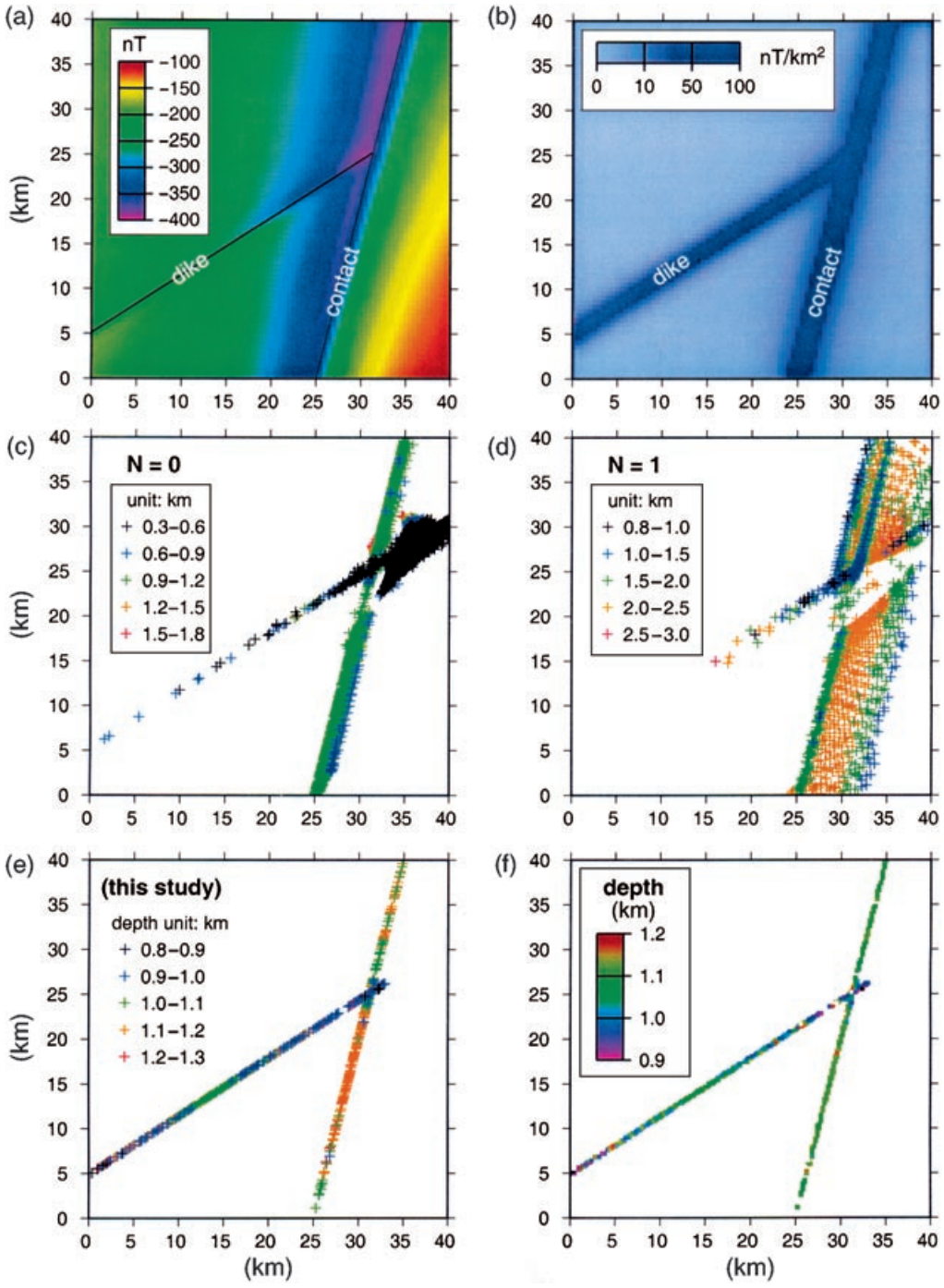

Figure 6 (a) Magnetic anomalies caused by a thin dike and a contact (or fault) model. The magnetization parameters are described in the text. The locations of the models are shown by black lines. (b) Amplitude distribution of the first-order analytic signal of the magnetic anomalies shown in (a). (c) The Euler's solutions of (a) calculated on the basis of the conventional Euler deconvolution method of Reid *et al.* (1990) with structural index $N = 0$. (d) The Euler's solutions of (a) calculated on the basis of the conventional Euler deconvolution method with structural index $N = 1$. Note that biased solutions are observed in both (c) and (d). (e) With the proposed method, the calculated locations and depths indicate the presence of the two structures very well. (f) The image view of the results in (e); the clustered depth solutions in each 0.5×0.5 grid cell are averaged.

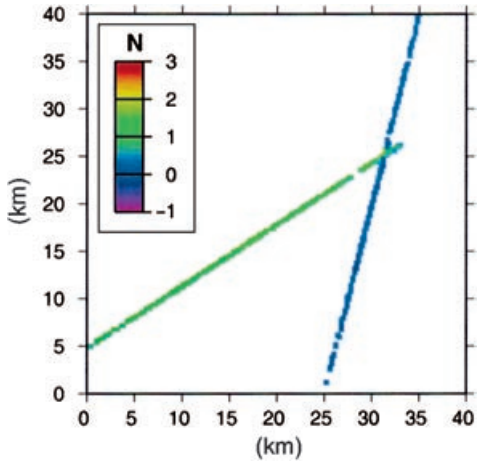

Figure 7 The images of the average structural indices clearly indicate the presence of a thin dike ($N \approx 1$) and a contact structure ($N \approx 0$) in Fig. 6(a).

Again, no selection criteria are adopted for the solutions. As we can see in Fig. 5(b), the good depth solutions cluster near the 'true' depth (i.e. 5 km) and the structural index solutions cluster at a value slightly less than zero. It can be seen that the good horizontal location is slightly mislocated to the west of the assumed distance (i.e. at 50 km) (compare Figs 1c and 5b). However, the discrepancy in horizontal distance is less than the grid interval of 0.5 km used here. When the noise component (amplitude) is less than about 10% of the magnetic anomaly, the tests show that good depth and structural index solutions cluster around the 'true' positions (i.e. depth $= 5$ km and $N = 0$). This test implies that the proposed method is especially good for imaging magnetic basements, which are usually corrupted by high-frequency anomalies.

3D model tests

A 3D model composed of a linear thin dike and a linear contact (or fault) (Fig. 6a) is used to examine the proposed method. The trend of the thin dike is oblique to the contact structure (Fig. 6a). The width of the thin dike is 0.2 km. The depth to the top of both the thin dike and the contact is 1 km. The magnetization is 1 A/m for both structures. The magnetization declination and inclination are -5° and 35°, respectively. A grid spacing of 0.2 km is used in the numerical calculation. The resultant (interfering) magnetic anomalies are shown in Fig. 6(a). Figure 6(b) shows the amplitude distribution of the first-order analytic signal (Hsu *et al.* 1996) of the magnetic anomalies shown in Fig. 6(a). The locations of the thin dike and the contact are clearly revealed by the distribution of the maximum amplitudes of the analytic signal (Fig. 6b). However, using only the maxima of the analytic signal, we are still unable to recognize the attributes of the underlying magnetic sources. The attributes of the magnetic sources may be obtained by comparing the amplitudes of different orders of analytic signal (e.g. Hsu *et al.* 1998; Smith *et al.* 1998).

For the conventional Euler deconvolution technique (Reid *et al.* 1990), the interfering magnetic anomalies are especially problematic when choosing a structural index. For example, in Fig. 6(a), if we use the conventional Euler deconvolution (Reid *et al.* 1990) and choose the structural index as zero (the theoretical value for a contact structure), 6086 valid solutions are obtained on the basis of a window of 5×5 grids and the acceptance level of 5% (Fig. 6c). As shown in Fig. 6(c), the location solutions are generally good for both models, whereas for the thin dike, the depth solutions are significantly underestimated. The incorrect solutions are especially concentrated near the junction area of the models (Fig. 6c). If the structural index is set at one (the theoretical value for a thin dike), 1772 valid solutions are obtained with the same criterion as for the structural index zero (Fig. 6d). However, the location solutions are diffuse and the depth solutions are biased. It can be seen that in this case, even though the correct structure index is used for the dike, its location and depth solutions are rather biased due to the interfering anomalies from the contact structure. In fact, the thin dike structure is not detected if the acceptance level of 1% is adopted for the above two cases.

In order to demonstrate the enhanced utility of the proposed method, a window of 4×4 grid nodes (i.e. 32 equations) is used to solve for the locations and structural indices. Using (2) and taking the orders $n = 1$ and $n = 2$, we obtain 690 valid solutions satisfying a tolerance (z_0/σ_z) greater than 20. The solutions are clustered and indicate clearly the locations and depths of both models (Fig. 6e). However, incorrect solutions also exist near the junction area (Fig. 6e). If we take into account the location image from the analytic signal amplitude (Fig. 6b), we can clearly discern the incorrect location solutions. To obtain an image view and a plausible depth estimation, the depth solutions in each grid column of 0.5×0.5 km^2 are averaged (Fig. 6f). In this case, the depth estimation errors for either the thin dike or the contact model are less than 15% in general. The images of the structural indices for the models are obtained in a similar manner (Fig. 7). Figure 7 clearly reveals the presence of the thin dike ($N \approx 1$) and the contact ($N \approx 0$) features (compare Fig. 7 and Table 1).

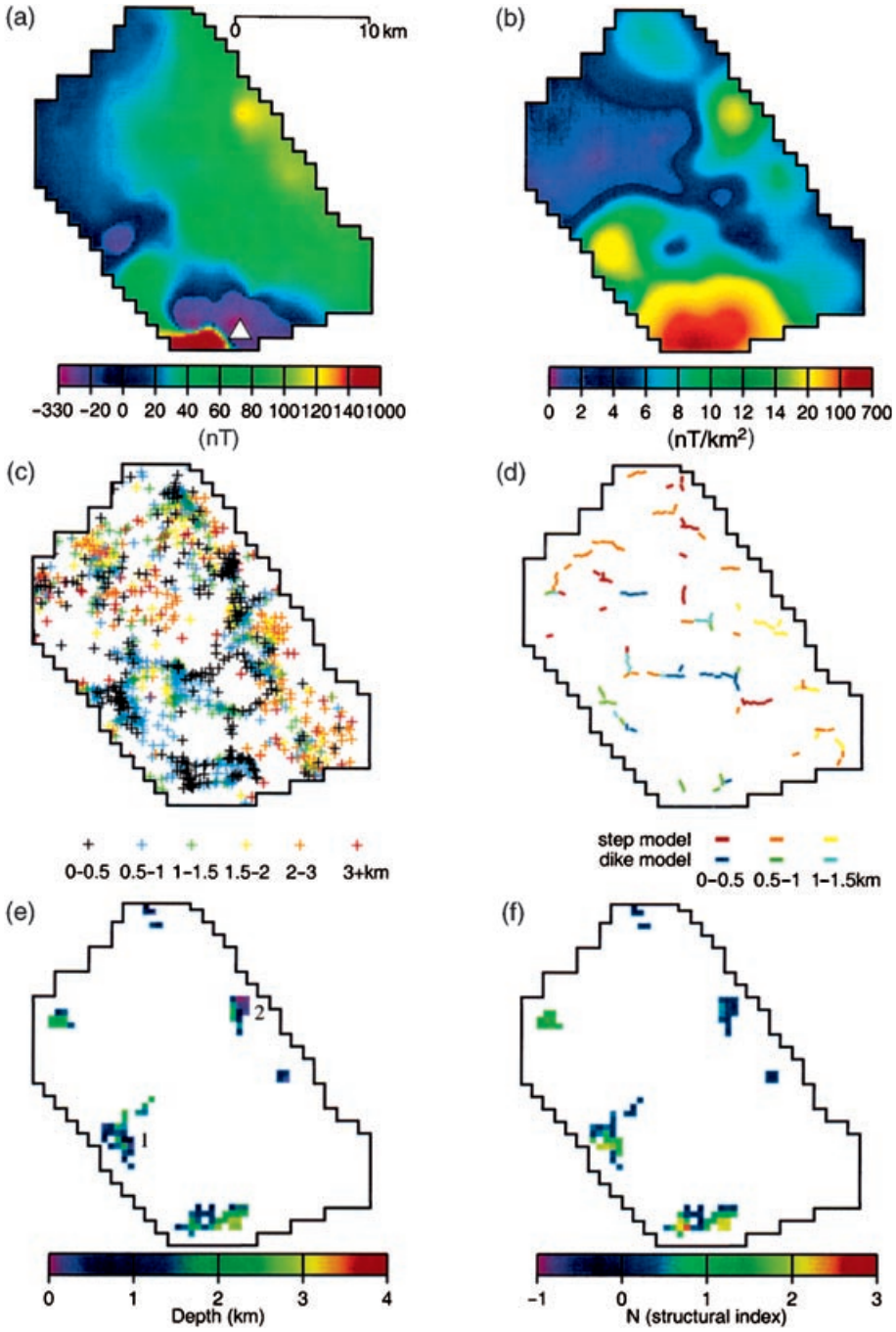

Figure 8 (a) Magnetic anomalies acquired in the nearshore of northern Taiwan (from Hsu *et al.* 1998). The white triangle marks a Pleistocene volcano. (b) Amplitude distribution of the first-order analytic signal of the magnetic anomalies as shown in (a). Note that the maximum amplitudes reveal the locations of magnetic sources. (c) The calculated locations and depths obtained using the conventional Euler deconvolution method of Reid *et al.* (1990). The structural index N is set at 0.5 and the window size is 7×7 grids. The solutions are obtained with an acceptance level of 3% (from Hsu *et al.* 1998). Note that the solutions are generally diffuse. (d) Calculated depths and possible structures from Hsu *et al.* (1998). (e) The calculated depths and their locations obtained using the present method. Note that the locations correspond perfectly with the maximum amplitudes in (b). (f) The structures, indicated by letters 1 and 2 in (e), have structural indices of near one and zero, respectively. The attributes of these two structures are in agreement with the structural types in (d), inferred from the amplitude ratio method of Hsu *et al.* (1998).

REAL DATA

For simplicity, in the real data example we use the magnetic data (Fig. 8a) used by Hsu *et al*. (1998). These magnetic data were acquired in the nearshore of northern Taiwan (see Figs 9 and 10 of Hsu *et al*. 1998). To ensure a stable calculation, the magnetic data were continued upwards for 800 m (Hsu *et al*. 1998). The geological context is described by Hsu *et al*. (1998). Based on the maximum amplitudes of the analytic signal (Fig. 8b), we can clearly discern the spatial distribution of causative magnetic sources. The valid solutions from the conventional Euler deconvolution method, though diffuse, are generally located around the maximum amplitudes of the analytic signal (compare Figs 8c and 8b). This is especially true for the shallow depth solutions (less than 1 km) whose locations correspond to the peaks of the analytic signal. However, from the conventional Euler deconvolution method, we cannot know the attributes of the causative sources.

If we use the proposed Euler method and adopt the same criteria as in the 3D model test, the locations of the magnetic sources agree well with the maximum amplitudes of the analytic signal (compare Figs 8e and 8b). The depth solutions are coherent with previous studies (compare Figs 8c–8e). For instance, looking at structure 1 in Fig. 8(e), we know that the possible depth to the sources is around 0.5 km. This depth solution is in agreement with the solutions shown in Figs 8(c) and 8(d). Moreover, the image of the structural index obtained for structure 1 suggests that structure 1 is probably a thin dike feature because its structural index is about one (compare Fig. 8f and Table 1). This result is similar to the result from the amplitude ratio method (compare Figs 8f and 8d). If we look at structure 2 in Fig. 8(e), it also has a similar depth to those in Figs 8(c) and 8(d). The structural index suggests that structure 2 is probably a contact or step-like feature (compare Fig. 8f and Table 1). This result is also consistent with the result from the amplitude ratio method (Hsu *et al*. 1998). Because of the use of a strict criterion, the solutions shown in Fig. 8(e,f) do not reveal the structures appearing in the middle part of Fig. 8(c) or Fig. 8(d). Those structures emerge when a looser criterion is used.

CONCLUSION

The structural index in the Euler deconvolution method can imply a magnetic source attribute. The structural index provides the position information of the calculated Euler depth solutions relative to the assumed causative model (Table 1). Thus, instead of assigning a structural index, this parameter should be estimated during Euler deconvolution. To achieve this purpose, I suggest using only the derivatives of the magnetic anomaly, through (2). With knowledge of the structural index, the interpretation of a magnetic source becomes easier and more significant for geophysicists and geologists. The estimation of structural index is especially important when interfering magnetic anomalies are present, implying that the use of a fixed structural index is not appropriate. If we use Euler's equation, via (2), to image the depths and attributes of magnetic sources, we obtain the following advantages.

1 The diffuse solutions from the conventional Euler deconvolution are considerably reduced; the valid solutions obtained locate the magnetic sources well. Consequently, the imaging of magnetic sources becomes meaningful.

2 Because we now have a structural index associated with each calculated depth, interpretation of the Euler depths becomes more significant.

3 Because the base level is eliminated, the numerical calculation becomes easier and we do not need to estimate the base level from some sophisticated approach.

4 The problem of interfering magnetic anomalies is significantly reduced because of the abandonment of a fixed structural index and the use of higher-resolution, higher-order derivatives of the magnetic anomalies. One should, however, pay attention to the amplification of the noise during numerical differentiation; this problem could be alleviated by upward continuation of the magnetic anomaly.

ACKNOWLEDGEMENTS

Discussion with Dr L.-Y. Chiao was very helpful. Constructive remarks and comments from Drs A.B. Reid, I. MacLeod, T. Dai, D. Ravat and one anonymous reviewer were appreciated. The figures were plotted using GMT software (Wessel and Smith 1998). This study was supported by the National Science Council, Republic of China.

REFERENCES

Atchuta Rao D., Ram Babu H.V. and Sanker Narayan P.V. 1981. Interpretation of magnetic anomalies due to dikes: the complex gradient method. *Geophysics* **46**, 1572–1578.

Barbosa V.C.F., Silva J.B.C. and Medeiros W.E. 1999. Stability analysis and improvement of structural index estimation in Euler deconvolution. *Geophysics* **64**, 48–60.

Debeglia N. and Corpel J. 1997. Automatic 3-D interpretation of potential field data using analytic signal derivatives. *Geophysics* **62**, 87–96, 1346.

Hansen R.O., Pawlowski R.S. and Wang X. 1987. Joint use of analytic signal and amplitude of horizontal gradient maxima for

three-dimensional gravity data interpretation. 57th SEG meeting, New Orleans, USA, Expanded Abstracts, 100–102.

Hsu S.-K., Coppens D. and Shyu C.-T. 1998. Depth to magnetic source using the generalized analytic signal. *Geophysics* **63**, 1947–1957.

Hsu S.-K., Sibuet J.-C. and Shyu C.-T. 1996. High-resolution detection of geologic boundaries from potential-field anomalies: an enhanced analytic signal technique. *Geophysics* **61**, 373–386.

Keating P.B. 1998. Weighted Euler deconvolution of the gravity data. *Geophysics* **63**, 1595–1603.

MacLeod I.N., Jones K. and Dai T.F. 1993. 3-D analytic signal in the interpretation of total magnetic field data at low magnetic latitudes. *Exploration Geophysics* **24**, 679–688.

Marson I. and Klingele E.E. 1993. Advantages of using the vertical gradient of gravity for 3-D interpretation. *Geophysics* **58**, 1588–1595.

Nabighian M.N. 1972. The analytic signal of two-dimensional magnetic bodies with polygonal cross-section: its properties and use for automated anomaly interpretation. *Geophysics* **37**, 507–517.

Nabighian M.N. 1974. Additional comments on the analytic signal of two-dimensional magnetic bodies with polygonal cross-section. *Geophysics* **39**, 85–92.

Nabighian M.N. 1984. Toward a three-dimensional automatic interpretation of potential field data via generalized Hilbert transforms: fundamental relations. *Geophysics* **49**, 957–966.

Ravat D. 1996. Analysis of the Euler method and its applicability in environmental magnetic investigations. *Journal of Environmental and Engineering Geophysics* **1**, 229–238.

Reid A.B., Allsop J.M., Granser H., Millett A.J. and Somerton I.W. 1990. Magnetic interpretation in three dimensions using Euler deconvolution. *Geophysics* **55**, 80–91.

Roest W.R., Verhoef J. and Pilkington M. 1992. Magnetic interpretation using the 3-D analytic signal. *Geophysics* **57**, 116–125.

Smith R.S., Thurston J.B., Dai T.-F. and MacLeod I.N. 1998. iSPI™ – the improved source parameter imaging method. *Geophysical Prospecting* **46**, 141–151.

Sundararajan N., Mohan N.L., Raghava M.S.V. and Seshagiri Rao S.V. 1985. Hilbert transform in the interpretation of magnetic anomalies of various components due to a thin infinite dike. *Pageoph* **123**, 557–566.

Thompson D.T. 1982. EULDPH: a new technique for making computer-assisted depth estimates from magnetic data. *Geophysics* **47**, 31–37.

Thurston J.B. and Smith R.S. 1997. Automatic conversion of magnetic data to depth, dip, and susceptibility contrast using the SPI (TM) method. *Geophysics* **62**, 807–813.

Wessel P. and Smith W.H.F. 1998. New improved, version of Generic Mapping Tools released. *EOS Transactions of the American Geophysical Union* **79**(47), 579.